2018

Modulation of apolipoprotein L1-microRNA-193a axis prevents podocyte dedifferentiation in high-glucose milieu

A. Mishra
Northwell Health

K. Ayasolla

V. Kumar
Northwell Health

X. Lan
Zucker School of Medicine at Hofstra/Northwell

H. Vashistha

See next page for additional authors

American Physiological Society | AMERICAN JOURNAL OF PHYSIOLOGY Renal Physiology

PUBLISHED ARTICLE
ARCHIVES
SUBSCRIPTIONS
SUBMISSIONS
CONTACT US

Am J Physiol Renal Physiol. 2018 May 1; 314(5): F832–F843.
Published online 2018 Jan 10.
doi: 10.1152/ajprenal.00541.2017: 10.1152/ajprenal.00541.2017

PMCID: PMC6031922
PMID: 29357419

Modulation of apolipoprotein L1-microRNA-193a axis prevents podocyte dedifferentiation in high-glucose milieu

Abheepsa Mishra,[1] Kamesh Ayasolla,[1] Vinod Kumar,[1] Xiqian Lan,[1] Himanshu Vashistha,[2] Rukhsana Aslam,[1] Ali Hussain,[1] Sheetal Chowdhary,[1] Shadafarin Marashi Shoshtari,[1] Nitpriya Paliwal,[1] Waldemar Popik,[3] Moin A. Saleem,[4] Ashwani Malhotra,[1] Leonard G. Meggs,[2] Karl Skorecki,[5] and Pravin C. Singhal[1]

[1]Center for Immunology and Inflammation, Feinstein Institute for Medical Research and Donald and Barbara Zucker School of Medicine at Hofstra/Northwell, Great Neck, New York

[2]Ochsner Clinic, New Orleans, Louisiana

[3]Meharry Medical College, Nashville, Tennessee

[4]Academic Renal Unit, University of Bristol, Bristol, United Kingdom

[5]Technion–Israel Institute of Technology and Rambam Health Care Campus, Haifa, Israel

Corresponding author.

Address for reprint requests and other correspondence: P. C. Singhal, Nephrology Div., 100 Community Dr., Great Neck, NY 11021 (e-mail: psinghal@northwell.edu).

Received 2017 Oct 31; Revised 2017 Dec 22; Accepted 2018 Jan 8.

Abstract

The loss of podocyte (PD) molecular phenotype is an important feature of diabetic podocytopathy. We hypothesized that high glucose (HG) induces dedifferentiation in differentiated podocytes (DPDs) through alterations in the apolipoprotein (APO) L1-microRNA (miR) 193a axis. HG-induced DPD dedifferentiation manifested in the form of downregulation of Wilms' tumor 1 (WT1) and upregulation of paired box 2 (PAX2) expression. WT1-silenced DPDs displayed enhanced expression of PAX2. Immunoprecipitation of DPD cellular lysates with anti-WT1 antibody revealed formation of WT1 repressor complexes containing Polycomb group proteins, enhancer of zeste homolog 2, menin, and DNA methyltransferase (DNMT1), whereas silencing of either WT1 or DNMT1 disrupted this complex with enhanced expression of PAX2. HG-induced DPD dedifferentiation was associated with a higher expression of miR193a, whereas inhibition of miR193a prevented DPD dedifferentiation in HG milieu. HG downregulated DPD expression of APOL1. miR193a-overexpressing DPDs displayed downregulation of APOL1 and enhanced expression of dedifferentiating markers; conversely, silencing of miR193a enhanced the expression of APOL1 and preserved DPD phenotype. Moreover, stably APOL1G0-overexpressing DPDs displayed the enhanced expression of WT1 but attenuated expression of miR193a; nonetheless, silencing of APOL1 reversed these effects. Since silencing of APOL1 enhanced miR193a expression as well as dedifferentiation in DPDs, it appears that downregulation of APOL1 contributed to dedifferentiation of DPDs through enhanced miR193a expression in HG milieu. Vitamin D receptor

agonist downregulated miR193a, upregulated APOL1 expression, and prevented dedifferentiation of DPDs in HG milieu. These findings suggest that modulation of the APOL1-miR193a axis carries a potential to preserve DPD molecular phenotype in HG milieu.

Keywords: APOL1, diabetic podocytopathy, high glucose, miR193a, podocyte dedifferentiation

INTRODUCTION

Podocytes play a key role in the maintenance of slit diaphragm, a component of the glomerular filtration barrier (5, 32, 33). Slit diaphragms are composed of several proteins expressed by podocytes and prevent leakage of plasma proteins (32, 33). An optimal expression of the slit diaphragm proteins is considered to be an integral part of podocyte health. Since both parietal epithelial cells (PECs) and podocytes (PDs) are derived from the same mesenchymal cells during embryogenesis (26, 37), injured adult podocytes go into dedifferentiation mode, reverting to the expression of PEC markers such as paired homeo box (PAX)-2 (26, 31, 39). High-glucose milieu has been demonstrated to induce dedifferentiation of PDs as a manifestation of PD injury (2, 16, 18, 37). However, the mechanisms involved are not clear.

PAX2 is a transcription factor that plays an important role in the development of kidneys (9–11, 38). In adult kidney, its expression is restricted to glomerular parietal and tubular epithelial cells (10). However, ectopic PAX2 expression in podocytes is a common finding in several pathological states including juvenile nephronophthisis (28), focal segmental glomerulosclerosis (30, 31), collapsing glomerulopathy (7), and diabetic glomerulosclerosis (2, 25). Since PAX2 is involved in cellular proliferation (43), this disease state expression may be an attempt by podocytes to regenerate in adverse milieus. In a mouse model of podocyte injury, evaluation of PD dedifferentiation in podocyte reporter mice demonstrated that PDs expressing PEC markers (PAX2/PAX8) far exceed PECs expressing PD markers (33).

MicroRNAs (miRs) are small, noncoding RNAs that negatively regulate gene expression at the posttranscription level (1). By an imperfect sequence complementation, miRNAs recognize and bind to the 3′-untranslated regions (3′-UTR) of target mRNAs, thereby inhibiting mRNA function through degradation, repression of translation, or both. Recently, miR193a has been demonstrated to induce downregulation of Wilms' tumor 1 (WT1) in podocytes (25). miR193a is tumor suppressor gene inducing apoptosis in podocytes through generation of oxidative stress. However, the role of miR193a in high-glucose-induced PD dedifferentiation has not been reported (29). Since WT1 inversely regulates PAX2 expression (8, 34), we hypothesize that high glucose would induce PAX2 expression through downregulation of WT1 and enhanced PD expression of miR193a.

Apolipoprotein (APO) L1 is a minor component of high-density lipoprotein complex and is expressed in kidney cells including podocytes, tubular cells, and other cell types (42). It is predominantly secreted by liver cells and circulates in the plasma (42). The G1 variant is a missense mutant haplotype (S342G:I384M), encoding two nonsynonymous amino acids, whereas the G2 variant is a 6-bp in-frame deletion resulting in loss of two amino acids (N388 and Y389) at the COOH-terminal helix of APOL1. Approximately 34% of African Americans carry one of the two risk variants, and 13% have some combination of both coding variants (41). Overt expression of APOL1G1 and -G2 has been associated with podocyte injury in both in vitro and in vivo studies (3, 15, 23, 24). The trypanolytic activity of circulating APOL1 (wild-type or G0) has been long appreciated and well-characterized, although the detailed molecular mechanism is not fully resolved (12). The function of APOL1G0 in podocytes is not clearly understood. We hypothesize that high glucose induces PD dedifferentiation through downregulation of APOL1 and upregulation of microRNA (miR) 193a. We further hypothesize that modulation of the APOL1-miR193a axis can be used as a tool to preserve PD differentiation in high-glucose milieu.

MATERIALS AND METHODS

Human podocytes. Human podocytes (PDs) were conditionally immortalized by introducing temperature-sensitive simian virus 40 T antigen by transfection (36). These cells proliferate at the permissive temperature (33°C) and enter growth arrest after transfer to the nonpermissive temperature (37°C). The growth medium contained RPMI 1640 supplemented with 10% fetal bovine serum (FBS), 1× penicillin-streptomycin, 1 mM L-glutamine, and 1× Insulin-Transferrin-Selenium (ITS; Invitrogen). Undifferentiated (UND) PDs were seeded on collagen-coated plates and differentiated through preincubation in normal RPMI (containing 11 mM glucose) for 10 days at 37°C (differentiated podocytes, DPDs). Before experimental protocols, DPDs were washed three times with glucose- and serum-free media. In experimental protocols, DPDs were incubated in media (glucose- and ITS-free RPMI) containing either normal glucose (5 mM) or high glucose (30 mM) for 48 h. DNA sequencing of these podocytes revealed APOL1G0 genotype.

Generation of a stable cell lines expressing APOL1G0 and vector. A stable cell line expressing *APOL1G0* was generated by retroviral infection as described previously (27). Briefly, the open reading frame of APOL1G0 was cloned into the retroviral vector pBABE carrying resistance to puromycin. To generate retroviral particles, the viral packaging cell line HEK-GP was cotransfected with the pBABE construct of interest and the vesicular stomatitis virus gene. UNDPDs were infected twice within 24 h with the viral-containing supernatant of HEK-GP cells. Selection with puromycin (1 μg/ml) was continued for 1 wk, and expression of the sequence of the *APOL1G0* was verified. Empty vector pBABE-eGFP was also transduced into UNDPDs to generate the control cell line.

Transfection of miR193a inhibitor and miR193a expression plasmid. miR193a inhibitor (25 nM; cat. no. 4464084; Thermo Fisher Scientific), miR193a expression plasmid (25 nM; cat. no. SC400232; OriGene), and empty vector (25 nM; pCMV-MIR; OriGene) were transfected in the cells using Lipofectamine 3000 Transfection Reagent (Thermo Fisher Scientific) according to the manufacturer's protocol. All miRNA products were dissolved in nuclease-free water. Briefly, DPDs were transfected at 70–80% confluence in six-well plates. The Lipofectamine transfection reagent (7.5 μl) and plasmid DNA were diluted in Opti-MEM (125 and 250 μl; Applied Biosystems, Thermo Fisher Scientific) followed by addition of P3000 Enhancer Reagent (10 μl) to diluted DNA. Diluted DNA (125 μl) was added to diluted Lipofectamine 3000 transfection reagent (125 μl) in the ratio of 1:1 (vol/vol) and incubated for 10 min at room temperature (25°C). After incubation, DNA-lipid complex was added to the cells and kept at 37°C in Opti-MEM for 48 h. Control and transfected cells were harvested for protein and RNA analyses.

Vitamin D receptor agonist treatment. Vitamin D receptor agonist (VDA; EB 1089, 10 nM; Tocris Bioscience) was used to modulate the expression of miR193a. VDA (2.2 mM) was initially dissolved in 10% DMSO (100 μl) and diluted further with sterile PBS buffer (pH 7.2) to achieve final working concentrations of 10 and 1 μM. The final concentration of DMSO was 0.1% in the vehicle in all of the experiments. DPDs in the experimental conditions were treated with VDA for 48 h and harvested for protein and RNA for further analyses.

Silencing of APOL1, WT1, and DNMT1. DPDs were transfected with scrambled small interfering RNA (siRNA; control) or APOL1 siRNA (20 nM; Santa Cruz Biotechnology), WT1 siRNA (25 nM; Santa Cruz Biotechnology), and DNA methyltransferase (DNMT1; 25 nM; Santa Cruz Biotechnology) with Lipofectamine RNAiMAX transfection reagent according to the manufacturer's protocol (Thermo Fisher Scientific). Briefly, DPDs were transfected at 60–80% confluence in six-well plates. Lipofectamine reagent (9 μl) and siRNAs (10 μM, 2–3 μl) were diluted in Opti-MEM (150 μl; Thermo Fisher Scientific). Then, diluted siRNA (150 μl) was added to diluted Lipofectamine reagent (150 μl) in 1:1 ratio (vol/vol) and incubated for 5 min at room temperature (25°C). After incubation, the siRNA-lipid complex was added to cells and kept at 37°C in Opti-MEM for 48 h. The cells were harvested for protein and RNA analyses. Control and transfected cells were used under control and experimental conditions.

RNA isolation and qPCR studies.

Total RNA was isolated from control and experimental DPDs with TRIzol reagent (Invitrogen). A 20-μl reaction mix was prepared containing iTaq Universal SYBR Green reaction mix (2×, 10 μl), iScript reverse transcriptase (0.25 μl), forward (fw) and reverse (rev) primers (2 μl), RNA (4 μl), and nuclease-free water (3.75 μl). Real-time PCR was performed using iTaq Universal SYBR Green One-Step Kit (Bio-Rad) according to the manufacturer's instructions using specific primers obtained from Thermo Fisher Scientific: *GAPDH*, fw 5′-CCC ATC ACC ATC TTC CAG GAG-3′, rev 5′-GTT GTC ATG GAT GAC CTT GGC-3′; *WT1*, fw 5′-CGAGAGCGATAACCACACAACG-3′, rev 5′-GTCTCAGATGCCGACCGTACAA-3′; *PAX2*, fw 5′-GGC TGT GTC AGC AAA ATC CTG-3′, rev 5′-TCC GGA TGA TTC TGT TGA TGG-3′; *APOL1*, fw 5′-ATC TCA GCT GAA AGC GGT GAAC-3′, rev 5′-TGA CTT TGC CCC CTC ATG TAAG-3′. The quantitative PCR (qPCR) conditions were as follows: 50°C for 10 min and 95°C for 1 min followed by 40 cycles of 95°C for 15 s and 60°C for 1 min. qPCR was performed using an ABI PRISM 7900HT Sequence Detection System, and relative quantification of gene expression was calculated using the comparative cycle threshold ($\Delta\Delta C_T$) method. Data were expressed as relative mRNA expression in reference to the control, normalized to the quantity of RNA input by performing measurements on an endogenous reference gene (GAPDH).

MicroRNA assay. For miRNA quantification, the total RNA was isolated from control and experimental DPDs with *mir*Vana miRNA Isolation Kit, and 1 μg of RNA was reverse-transcribed using miR193a- and spliceosomal U6 small nuclear RNA-specific RT primers to generate first-strand cDNA from mRNA using *Taq*Man MicroRNA Reverse Transcription Kit (Thermo Fisher Scientific) according to manufacturer's instructions. For cDNA, a 15-μl PCR reaction was prepared containing 100 mM dNTP mix (0.15 μl), 50 U/μl MultiScribe RT enzyme (1 μl), 10× RT buffer (1.5 μl), 20 U/μl RNase inhibitor (0.19 μl), nuclease-free water (4.16 μl), RNA (5 μl), and primers (3 μl). The PCR condition was as follows: 16°C for 30 min, 42°C for 30 min, 85°C for 5 min, and 4°C until stopped. Real-time PCR was performed by using *Taq*Man-based PCR Master Mix and detection primers miR193a and spliceosomal U6 small nuclear RNA (Thermo Fisher Scientific) in Applied Biosystems 7500. For real-time PCR, a 10-μl reaction mix was prepared containing *Taq*Man PCR Master Mix II (5 μl), cDNA (2 μl), nuclease-free water (2 μl), and primer (1 μl). The qPCR conditions were as follows: 50°C for 2 min and 95°C for 10 min followed by 40 cycles of 95°C for 15 s and 60°C for 1 min. U6 was used as an internal control. Relative quantification of gene expression was calculated using the $\Delta\Delta C_T$ method, and the results were normalized to spliceosomal U6 small nuclear RNA expression.

Immunofluorescence detection of APOL1. Control and experimental podocytes were fixed and permeabilized with a buffer containing 0.02% Triton X-100 and 4% formaldehyde in PBS. Fixed cells were washed three times in PBS and blocked in 10% BSA for 60 min at 37°C. Subsequently, cells were labeled with anti-APOL1 (Proteintech). 4′,6′-Diamidino-2-phenylindole was used for nuclear localization. Control and experimental cells were examined under immunofluorescence microscope.

Western blotting studies. Western blotting studies were carried out as described previously (4, 17, 22). Briefly, control and experimental cells were harvested and lysed in RIPA buffer containing 50 mM Tris·HCl (pH 7.5), 150 mM NaCl, 1 mM EDTA, 1% Nonidet P-40, 0.25% deoxycholate, 0.1% SDS, 1× protease inhibitor cocktail (Cocktail Set I; Calbiochem), 1 mM PMSF, and 0.2 mM sodium orthovanadate. Protein concentration was measured using Bio-Rad Protein Assay Kit. Total protein lysed extracts (30 μg/lane) were loaded on a 10% polyacrylamide (PAGE) premade gel (Bio-Rad) and transferred onto polyvinylidene difluoride membranes processed for immunostaining with primary antibodies against APOL1 (mouse monoclonal, 1:1,000; Proteintech), WT1 (rabbit polyclonal, 1:1,000; Abcam), PAX2 (rabbit polyclonal, 1:800; Abcam), menin (mouse monoclonal, 1:1,000; Santa Cruz Biotechnology), DNMT1 (mouse monoclonal, 1:1,000; Santa Cruz Biotechnology), enhancer of zeste homolog 2 (EZH2; goat polyclonal, 1:1,000; Santa Cruz Biotechnology), retinoblastoma binding protein 4 (RBBP4; rabbit polyclonal, 1:1,000; Santa Cruz Biotechnology), Tri-Methyl-Histone H3 (Lys27; H3K27me3; rabbit polyclonal, 1:1,000; Cell Signaling Technology), podocalyxin (rabbit polyclonal, 1:1,000; Thermo Fisher

Scientific), and nephrin (rabbit polyclonal, 1:800; Abcam) followed by treatment with horseradish peroxidase-labeled appropriate secondary antibodies. The blots were developed using a chemiluminescence detection kit (Pierce, Rockford, IL) and exposed to X-ray film (Eastman Kodak, Rochester, NY). Equal protein loading and the protein transfer were confirmed by immunoblotting for determination of actin/GAPDH protein using a polyclonal β-actin/GAPDH antibody (Santa Cruz Biotechnology) on the same (stripped) Western blots.

Immunoprecipitation. Lysates from undifferentiated and differentiated PDs were first immunoprecipitated following the addition of 5 μg of monoclonal antibody to WT1 (Santa Cruz Biotechnology). The immune complexes were then collected using 25 μl of Protein A and G Sepharose beads (GE Healthcare Life Sciences) in RIPA buffer. The immunoprecipitation (IP) was carried out at 4°C, for 4 h, on a rotating platform. After this, precipitated A/G proteins were pelleted down by centrifugation at 4,500 rpm for 10 min at 4°C. Next, the protein pellet was washed (3×) each time with 1 ml of cold RIPA lysis buffer followed by centrifugation each time for 10 min at 2,500 rpm in a microfuge. After washings, beads were resuspended in 100 μl of lysis buffer to which SDS-PAGE sample buffer (50 μl) was added, and samples were boiled at 100°C followed by SDS-PAGE and immunoblotted using specific antibodies as indicated.

Statistical analyses. Statistical comparisons were performed with the program Prism using the Mann-Whitney *U* test for nonparametric data and the unpaired *t*-test for parametric data. A P value <0.05 was accepted as statistically significant.

RESULTS

High glucose causes dedifferentiation of podocytes. Dedifferentiation of PDs is characterized by enhanced expression of PAX2 and downregulation of WT1. To determine the effect of high glucose on PAX2 expression, proteins and RNAs were extracted from control and high-glucose-treated DPDs ($n = 3$). Protein blots were probed for PAX2 and reprobed for actin. Gels from three different lysates are displayed in Fig. 1*A*, *top*. Cumulative densitometric data are shown in bar graphs (Fig. 1*A*, *bottom*). High glucose enhanced ($P < 0.05$) expression of PAX2 in DPDs. cDNAs were amplified with a specific primer for PAX2. Cumulative data on mRNA expression of PAX2 are shown in Fig. 1*C*. High glucose also enhanced PAX2 mRNA expression in DPDs. Protein blots of the same lysate preparations were probed for WT1 and reprobed for actin. Gels from three different lysates are displayed in Fig. 1*B*, *top*. Cumulative densitometric data are shown as a bar graph in Fig. 1*B*, *bottom*. cDNAs were amplified with a specific primer for WT1. Cumulative data are shown in a bar graph (Fig. 1*D*). High glucose downregulated ($P < 0.05$) WT1 mRNA as well as protein expression in DPDs. These findings suggest that high glucose downregulates transcription and translation of WT1 but enhances transcription of PAX2 in DPDs.

We examined whether there is a causal relationship between high-glucose-induced downregulation of WT1 and upregulation of PAX2 expression in DPDs. DPDs were transfected with either scrambled or WT1 siRNA ($n = 3$). Subsequently, protein blots were probed for WT1 and reprobed for PAX2 and GAPDH. Gels from three different lysates are displayed in Fig. 1*E*. Cumulative densitometric data are shown in Fig. 1*F*. DPDs silenced for WT1 displayed enhanced ($P < 0.05$) PAX2 expression. These findings confirm that downregulation of WT1 causes upregulation of PAX2 in DPDs.

High glucose induces DPD dedifferentiation through upregulation of miR193a. Since miR193a is a negative regulator of WT1 in PDs (11), we asked whether high glucose is downregulating WT1 via upregulation of miR193a. DPDs were incubated in media containing either normal glucose (control; 5 mM) or high glucose (30 mM) for 48 h ($n = 3$). RNAs were extracted and assayed for miR193a. As shown in Fig. 2*A*, high glucose enhanced expression of miR193a in DPDs.

To determine whether a specific miR193a inhibitor carries the potential to reverse the effect of high-glucose milieu, DPDs were incubated in media containing normal glucose (5 mM; control), high glucose (30 mM), or empty vector (pCMV-MIR; 25 nM) with or without miR193a inhibitor (25 nM; Applied

Biosystems, Thermo Fisher Scientific) for 48 h followed by RNA extraction. RNAs were assayed for miR193a. High glucose enhanced ($P < 0.01$) the expression of miR193a in DPDs; however, this effect of high glucose was attenuated by inhibition of miR193a (Fig. 2*B*).

We hypothesized that if high glucose induced dedifferentiation of DPDs through upregulation of miR193a, then inhibition of miR193a in high-glucose milieu would preserve DPD molecular phenotype. DPDs were incubated in media containing normal glucose (control; 5 mM), high glucose (30 mM), or empty vector (pCMV-MIR; 25 nM) with or without a specific inhibitor of miR193a (25 nM) for 48 h ($n = 3$). Proteins were extracted, and protein blots were probed for WT1 and reprobed for PAX2 and actin. Gels are displayed in Fig. 2*C*. Cumulative densitometric data are shown as a bar diagram in Fig. 2*D*. High glucose decreased ($P < 0.05$) DPD expression of WT1 and enhanced ($P < 0.05$) expression of PAX2. However, miR193a inhibitor prevented upregulation of PAX2 in high-glucose milieu. These findings confirm that high glucose induces dedifferentiation of DPDs through upregulation of miR193a.

High glucose downregulates DPD expression of APOL1 through upregulation of miR193a. To determine the dose-response effect of high glucose on APOL1 expression in DPDs, cells were incubated in media containing variable concentrations of glucose (5, 10, 20, 30, and 35 mM) for 48 h ($n = 3$). Protein blots were probed for APOL1 and reprobed for GAPDH. Representative gels are displayed in Fig. 3*A*. Glucose downregulated APOL1 expression in DPDs at higher concentrations (≥30 mM).

To evaluate the APOL1 relationship with dedifferentiation markers, UNDPDs, DPDs treated with RPMI containing either conventional glucose (11 mM) or high glucose (30 mM) for 48 h, were analyzed for dedifferentiation markers ($n = 4$). Protein blots were probed for APOL1 and reprobed for WT1, PAX2, and GAPDH. Gels of three different lysates are displayed in Fig. 3*B*. Cumulative densitometric data are shown as a bar diagram (Fig. 3*C*). DPDs displayed the expression of APOL1 and WT1 but attenuated expression of PAX2; on the other hand, high glucose inhibited the expression of APOL1 and WT1 but enhanced the expression PAX2. These findings suggest that downregulation of APOL1 in DPDs is temporally associated with downregulation of WT1 and upregulation of PAX2 in high-glucose milieu.

To determine whether miR193a is regulating the expression of APOL1, DPDs were incubated in media containing normal glucose (5 mM), high glucose (30 mM), or empty vector (25 nM; pCMV-MIR) with or without miR193a inhibitor (25 nM) for 48 h ($n = 3$). Proteins and RNAs were extracted. Protein blots were probed for APOL1 and reprobed for GAPDH. Gels are displayed in Fig. 3*D*. Cumulative densitometric data are shown in bar graphs (Fig. 3*E*). High glucose downregulated ($P < 0.05$) APOL1 expression in DPDs; however, miR193a inhibitor enhanced ($P < 0.05$) APOL1 expression in high-glucose milieu. RNAs were extracted from the lysates of Fig. 3*D*, and cDNAs were amplified with a specific primer for *APOL1*. Cumulative data are shown as a bar diagram (Fig. 3*F*). High glucose downregulated *APOL1* mRNA expression; however, inhibition of miR193a stimulated *APOL1* mRNA expression both in control and high-glucose milieus. These findings suggest that miR193a negatively regulates APOL1 expression in DPDs under control as well as in high-glucose milieus.

DPDs grown on coverslips were incubated in media containing either normal glucose (5 mM) or high glucose (30 mM) with or without a miR193a inhibitor (miR; 25 nM) for 48 h ($n = 3$) followed by immunolabeling for APOL1. Subsequently, cells were examined under a confocal microscope. Representative fluoromicrographs are shown in Fig. 3*G*. High glucose downregulated APOL1 expression (green fluorescence) in DPDs; however, this effect of high glucose was mitigated by inhibition of miR193a.

To determine the effect of overexpression of miR193a on APOL1 expression, DPDs were transfected with either empty vector or miR193a plasmid ($n = 3$). Proteins and RNAs were extracted. Protein blots were probed for WT1, PAX2, and APOL1 and reprobed for GAPDH. Gels from three different lysates are displayed in Fig. 4*A*. Cumulative densitometric data are shown as a bar diagram in Fig. 4*B*. miR193a-overexpressing DPDs showed downregulation of APOL1 and WT1 but upregulation of PAX2. cDNAs

were amplified for *APOL1*. Cumulative data are shown in a bar diagram (Fig. 4*C*). DPDs overexpressing miR193a showed downregulation of *APOL1* mRNA. These findings confirm that miR193a negatively regulates expression of APOL1 in DPDs.

WT1 repressor complex preserves DPD molecular phenotype. To characterize the molecular phenotypes of undifferentiated (UND) and differentiated PDs (DPD), protein blots of UNDPDs (0-day incubation) and DPDs (10-day incubation) were probed for PDs (nephrin and podocalyxin), PEC (PAX2) markers, APOL1, components of WT1 repressor complex (RBBP4, EZH2, menin, H3K27me3, and DNMT1), and actin. Gels from three different lysates are displayed in Fig. 5*A* (PD and PEC markers) and Fig. 5*B* (components of WT1 repressor complex, input for IP data). Cumulative densitometric data from the lysates of Fig. 5, *A* and *B*, are shown as bar diagrams (Fig. 5, *C* and *D*). DPDs (10-day incubation) displayed higher expression of APOL1, nephrin, and podocalyxin but lower expression of PAX2 compared with undifferentiated PDs (0-day; Fig. 5, *A* and *C*). Interestingly, DPDs (10-day incubation) displayed enhanced expression of the components of WT1 repressor complex (Fig. 5, *B* and *D*).

To confirm the composition of WT1 repressor complex, input lysates of UND and DPD were immunoprecipitated (IP) with the anti-WT1 antibody. IP fractions were probed for WT1, RBBP4 (Polycomb group protein), EZH2, menin, H3K27me3, DNMT1, and IgG. Gels from three different IP fractions are displayed in Fig. 5*E*. Cumulative densitometric data from the lysates are shown in bar graphs (Fig. 5*F*). IP fractions of DPDs displayed enhanced expression of WT1, RBBP4, menin, EZH2, H3K27me3, and DNMT1 compared with 0-day PDs. These findings confirm that WT1 repressor complex is composed of WT1, RBBP4, menin, EZH2, H3K27me3, and DNMT1.

We asked whether the integrity of WT1 repressor complex is critical for the prevention of dedifferentiation of DPDs. DPDs were transfected with scrambled, WT1 siRNA, DNMT1 siRNA, or WT1 + DNMT1 siRNAs. After 48 h, protein blots were probed for PAX2, WT1, nephrin, podocalyxin, and DNMT1 and reprobed for actin. Gels from three different lysates are displayed in Fig. 5*G*. Cumulative densitometric data are shown as a bar diagram in Fig. 5*H*. Lack of either WT1 or DNMT1 enhanced the expression of PAX2. Interestingly, combined silencing of WT1 and DNMT1 displayed additive effect on PAX2 expression. These findings suggest that disruption of WT1 repressor complexes derepresses the expression of PAX2.

Role of APOL1 in preservation of DPD molecular phenotype. To determine the role of APOL1 in the preservation of the DPD molecular phenotype, DPDs were transfected with either control (scrambled) or APOL1 siRNA. Proteins were extracted from control and transfected cells ($n = 3$). Protein blots were probed for APOL1 and reprobed for PAX2, WT1, and GAPDH. Gels from three different lysates are displayed in Fig. 6*A*. Cumulative densitometric data are shown in a bar diagram (Fig. 6*B*). APOL1-silenced DPD displayed attenuated ($P < 0.05$) expression of WT1 and enhanced ($P < 0.05$) expression of PAX2 compared with control and scrambled DPDs. These findings indicate that APOL1 expression is critical for the preservation of DPD molecular phenotype.

To determine whether APOL1 would be preserving DPD molecular phenotype through alterations in miR193a expression, DPDs were transfected with either control (scrambled) or APOL1 siRNA. RNAs were extracted from control and transfected cells ($n = 3$). RNAs were assayed for miR193a. Cumulative data are shown in a bar diagram (Fig. 6*C*).

To establish a functional relationship between miR193a and APOL1, DPDs were transfected with either control (scrambled) or APOL1 siRNA and incubated in media with or without miR193a inhibitor (25 nM) for 48 h ($n = 3$). Protein blots were probed for APOL1, WT1, PAX2, and GAPDH. Gels from three different lysates are displayed in Fig. 6*D*. Silencing of APOL1 in DPDs downregulated WT1 and enhanced the expression of PAX2; however, inhibition of miR193a did not alter this effect of APOL1. These findings suggest the importance of APOL1 expression to sustain the functionality of the APOL1-miR193a axis.

To determine whether miR193a inhibitor is fully functional in APOL1-silenced PDs, RNAs were extracted from the lysates of Fig. 6*D*. RNAs were assayed, and cumulative data ($n = 3$) are shown in a bar diagram (Fig. 6*E*). miR193a inhibitor downregulated PD expression of miR193a in control conditions but could not do so in APOL1-silenced PDs. These findings suggest that APOL1 is required for the functionality of the APOL1-miR193a axis in DPDs.

APOL1 negatively regulates miR193a expression in DPDs. To confirm a relationship between APOL1 and miR193a, UNDPDs stably expressing vector and overexpressing APOL1G0 were differentiated (incubation in RPMI containing 11 mM glucose for 10 days). APOL1G0-expressing DPDs were transfected with either scrambled or APOL1 siRNAs ($n = 6$). After 48 h, proteins and RNAs were extracted. Protein blots were probed for APOL1 and reprobed for WT1, PAX2, and actin. Gels from three different lysates are displayed in Fig. 7*A*. Cumulative densitometric data ($n = 6$) are shown as a bar diagram (Fig. 7*B*). DPDs overexpressing APOL1G0 displayed enhanced expression of APOL1 and WT1 but downregulation of PAX2; however, silencing of APOL1 reversed this APOL1G0. RNAs were assayed for miR193a, and cumulative data are shown as a bar diagram (Fig. 7*C*). DPDs overexpressing APOL1G0 displayed downregulation of miR193a expression; however, silencing of APOL1 upregulated the expression of miR193a. These findings confirm that APOL1 negatively controls the expression of miR193a.

Vitamin D receptor agonist preserves DPD phenotype through modulation of the miR193a-APOL1 axis in high-glucose milieu.
Vitamin D_3 has been known to downregulate expression of miR193a in parietal epithelial cells (20). To determine the effect of VDA on miR193a expression in UNDPDs, UNDPDs were incubated in media containing either vehicle (0.1% DMSO) alone or different concentrations of VDA (EB 1089; 0, 1.0, 10.0, and 100.0 nM) for 48 h ($n = 3$). RNAs were extracted and assayed for miR193a. Cumulative data are shown in a bar diagram (Fig. 8*A*). VDA downregulated miR193a in UNDPDs in a dose-dependent manner.

To determine the effect of VDA on high-glucose-induced modulation of miR193a, DPDs were incubated in media containing normal glucose (5 mM), high glucose (30 mM), or vehicle (0.1% DMSO) with or without VDA (EB 1089; 10 nM) for 48 h ($n = 3$). RNAs were extracted and assayed for miR193a. Cumulative data are shown as a bar diagram (Fig. 8*B*). High glucose enhanced ($P < 0.01$) expression of miR193a in DPDs. However, VDA inhibited high-glucose-induced upregulation of DPD expression of miR193a.

To examine the effect of VDA on high-glucose-induced downregulation of APOL1, DPDs were incubated in media containing either normal glucose (5 mM) or high glucose (30 mM) with or without VDA (EB 1089; 10 nM) for 48 h ($n = 3$). Protein blots were probed for APOL1 and reprobed for GAPDH. Representative gels are displayed in Fig. 8*C*. Cumulative densitometric data are shown in a bar diagram (Fig. 8*D*). High glucose downregulated ($P < 0.05$) APOL1 expression in DPDs; however, VDA enhanced APOL1 expression in high-glucose milieu. These findings suggest that VDA has potential to preserve DPD expression of APOL1 in high-glucose milieu.

To evaluate the effect of VDA on high-glucose-induced dedifferentiation, DPDs were incubated in media containing normal glucose (5 mM), vehicle (0.1% DMSO), or high glucose (30 mM) with or without VDA (EB 1089; 10 nM) for 48 h ($n = 3$). Protein blots were probed for WT1 and PAX2 and reprobed for GAPDH. Representative gels are displayed in Fig. 8*E*. Cumulative densitometric data are shown in a bar diagram (Fig. 8*F*). High glucose downregulated ($P < 0.05$) DPD expression of WT1 but enhanced ($P < 0.05$) the expression of PAX2. However, VDA enhanced the expression of WT1 under high-glucose milieu. Moreover, VDA downregulated high-glucose-induced PAX2 expression in DPDs. These findings suggest that VDA carries a potential to preserve DPD molecular profile in high-glucose milieu.

DISCUSSION

The present study demonstrated that high glucose induced dedifferentiation in DPDs. High glucose enhanced PAX2 expression, a marker of podocyte dedifferentiation, as a consequence of disruption of WT1 repressor complex. High-glucose-induced DPD dedifferentiation was associated with a higher expression of miR193a and inhibition of miR193a prevented DPD dedifferentiation. DPDs overexpressing miR193a displayed downregulation of APOL1 and enhanced expression of dedifferentiating markers; conversely, silencing of miR193a enhanced the expression of APOL1 and also preserved DPD phenotype. Interestingly, high glucose also attenuated DPD expression of APOL1. Moreover, stably APOL1G0-overexpressing DPDs displayed the enhanced expression of WT1 but attenuated expression of miR193a; nonetheless, silencing of APOL1 reversed these effects. Since silencing of APOL1 enhanced miR193a expression as well as dedifferentiation in DPDs, it appears that downregulation of APOL1 contributed to enhanced miR193a expression in high-glucose milieu. Vitamin D receptor agonist (VDA) downregulated miR193a, upregulated APOL1 expression, and prevented dedifferentiation of DPDs in high-glucose milieu. These findings suggest a novel role of APOL1 in the preservation of molecular phenotype of DPDs in high-glucose milieu.

Expression of parietal epithelial proteins such as claudin 1 and PAX2 in the glomerular capillary tufts in diabetic nephropathy could be a consequence of the replacement of PDs by PECs or the reversal of PDs to PECs phenotype. Chen et al. (6) demonstrated that high-glucose milieu enhanced PAX2 gene expression in mouse embryonic mesenchymal epithelial cells and kidney explants. In an experimental model of podocyte reporter mice, podocyte injury stimulated expression of PAX2 (34). Therefore, expression of PAX2 by glomerular capillary epithelial cells may not be able to predict their lineage.

WT1 has been reported to regulate PAX2 expression negatively through the formation of a repressor complex (44). WT1 repressor complex containing Polycomb group proteins, EZH2, and menin binds at PAX2 gene and has been demonstrated to decrease transcription of PAX2 (40, 44). In the present study, high glucose downregulated WT1 and decreased the transcription of PAX2 in DPDs. WT1-bound IP fraction revealed the presence of Polycomb group protein, EZH2, menin, and DNMT1. Silencing of WT1 or DNMT1 disrupted the repressor complex and upregulated PAX2 expression in DPDs. These findings suggest that high-glucose-induced downregulation of WT1 and enhanced PAX2 expression occurred through disruption of WT1 repressor complex. We have displayed proposed composition of WT1 repressor complex on PAX2 in Fig. 9*A*. However, these observations need to be confirmed in in vivo studies.

miR193a has been demonstrated to regulate WT1 transcription inversely in podocytes (14). miR193a transgenic mice displayed loss of WT1 by podocytes and developed focal glomerular sclerosis (14). Notably, dedifferentiation of PDs in the form of PAX2 expression was not studied in this model. In the present study, high glucose enhanced expression of miR193a and downregulated WT1 expression in the podocytes. Inhibition of miR193a caused upregulation of podocyte WT1 expression in high-glucose milieu, suggesting an inverse relationship between miR193a and WT1 in high-glucose milieu. Moreover, inhibition of miR193a upregulated PD expression of WT1 and downregulated PAX2 expression in high-glucose milieu. These findings suggest that modulation of miR193a could be used as a therapeutic strategy to preserve podocyte molecular integrity in high-glucose milieu.

In the present study, high-glucose-induced upregulation of miR193a displayed a temporal relationship with downregulation of APOL1 expression in PDs. On the other hand, APOL1-silenced PDs displayed upregulation of miR193a, and overexpressing APOL1 PDs showed downregulation of miR193a expression. These findings suggest a negative feedback relationship between APOL1 and miR193a in PDs. As noted below, this miR193a-mediated downregulation of APOL1 in high-glucose milieu could provide an explanation for the low or absence of any association of APOL1 renal risk variants with diabetic kidney disease (13). On the other hand, downregulation of APOL1 was associated with dedifferentiation of DPDs both in high-glucose milieu as well as under control conditions, whereas upregulation of APOL1 provided protection against dedifferentiation of podocytes in high-glucose milieu. Therefore, enhanced APOL1

expression could be considered with caution as a strategy to preserve podocyte phenotype in high glucose or related adverse milieus. However, in the absence of such adverse milieus, it is considered that APOL1 expression may be dispensable to kidney health (19).

Since LPS, TNF-α, human immunodeficiency virus, and IFN-γ have been reported to enhance expression of APOL1 in podocytes (23, 24, 27), these agents could be used to prevent downregulation of APOL1 in high-glucose milieu. However, these agents are phlogogenic de novo and would not be suitable in chronic kidney disease-carrying pre-existing inflammatory milieu. In our study, we observed that VDA not only downregulated miR193a, but also enhanced PD expression of APOL1 in high-glucose milieu. Therefore, VDA could be used to provide protection against dedifferentiation in high-glucose milieu through enhanced PD expression of APOL1. However, using VDA for increasing APOL1 in high-glucose milieu would be detrimental for PD health if the host carries APOL1 risk alleles (3, 15, 23, 24). Therefore, it would be mandatory to characterize the genetic profile of APOL1 before using VDA as a therapeutic strategy to preserve PD molecular phenotype in high-glucose milieu.

Genetic epidemiology indicated that African Americans carrying APOL1 risk alleles (G1 and G2) are prone to develop chronic kidney diseases at higher rates with few exceptions such as diabetic nephropathy compared with European Americans (13, 21, 41). In the present study, high-glucose milieu downregulated expression of APOL1 in podocytes; therefore, high-glucose milieu would also downregulate podocyte expression of APOL1 risk alleles in African Americans carrying APOL1 risk alleles. Since enhanced expression of APOL1 risk alleles has been reported to be cytotoxic to podocytes, downregulation of APOL1 risk alleles in high-glucose milieu is unlikely to modulate net outcome. Therefore, our data are consistent with the epidemiological observations (13).

We conclude that high-glucose-induced upregulation of miR193a stimulated attenuated expression of APOL1 manifesting in the form of DPD dedifferentiation (Fig. 9*B*). This effect of high glucose could be prevented by VDA through the reversal of APOL1-miR193 axis alterations.

GRANTS

This work was supported by National Institute of Diabetes and Digestive and Kidney Diseases Grants R01-DK-098074, R01-DK-084910, and R01-DK-083931 (to P. C. Singhal), Israel Science Foundation Grant 890015, and the Ernest and Bonnie Beutler Research Program of Excellence in Genomic Medicine of the Rambam Health Care Campus.

DISCLOSURES

No conflicts of interest, financial or otherwise, are declared by the authors.

AUTHOR CONTRIBUTIONS

P.C.S. conceived and designed research; A. Mishra, V.K., X.L., H.V., R.A., A.H., S.C., S.M.S., and N.P. performed experiments; A. Mishra, K.A., V.K., X.L., and A. Malhotra analyzed data; W.P., M.A.S., A. Malhotra, L.G.M., and K.S. interpreted results of experiments; A. Mishra, K.A., and H.V. prepared figures; P.C.S. drafted manuscript; A. Mishra, K.A., V.K., X.L., H.V., R.A., A.H., S.C., S.M.S., N.P., W.P., M.A.S., A. Malhotra, L.G.M., K.S., and P.C.S. approved final version of manuscript.

REFERENCES

1. Ambros V. microRNAs: tiny regulators with great potential. Cell 107: 823–826, 2001. doi:10.1016/S0092-8674(01)00616-X. [PubMed: 11779458] [CrossRef: 10.1016/S0092-8674(01)00616-X]

2. Andeen NK, Nguyen TQ, Steegh F, Hudkins KL, Najafian B, Alpers CE. The phenotypes of podocytes and parietal epithelial cells may overlap in diabetic nephropathy. Kidney Int 88: 1099–1107, 2015. doi:10.1038/ki.2015.273. [PMCID: PMC4653076] [PubMed: 26376129] [CrossRef: 10.1038/ki.2015.273]

3. Beckerman P, Bi-Karchin J, Park AS, Qiu C, Dummer PD, Soomro I, Boustany-Kari CM, Pullen SS, Miner JH, Hu CA, Rohacs T, Inoue K, Ishibe S, Saleem MA, Palmer MB, Cuervo AM, Kopp JB, Susztak K. Transgenic expression of human APOL1 risk variants in podocytes induces kidney disease in mice. Nat Med 23: 429–438, 2017. doi:10.1038/nm.4287. [PMCID: PMC5603285] [PubMed: 28218918] [CrossRef: 10.1038/nm.4287]

4. Chandel N, Husain M, Goel H, Salhan D, Lan X, Malhotra A, McGowan J, Singhal PC. VDR hypermethylation and HIV-induced T cell loss. J Leukoc Biol 93: 623–631, 2013. doi:10.1189/jlb.0812383. [PMCID: PMC3597838] [PubMed: 23390308] [CrossRef: 10.1189/jlb.0812383]

5. Charest PM, Roth J. Localization of sialic acid in kidney glomeruli: regionalization in the podocyte plasma membrane and loss in experimental nephrosis. Proc Natl Acad Sci USA 82: 8508–8512, 1985. doi:10.1073/pnas.82.24.8508. [PMCID: PMC390945] [PubMed: 3866237] [CrossRef: 10.1073/pnas.82.24.8508]

6. Chen YW, Liu F, Tran S, Zhu Y, Hébert MJ, Ingelfinger JR, Zhang SL. Reactive oxygen species and nuclear factor-kappa B pathway mediate high glucose-induced Pax-2 gene expression in mouse embryonic mesenchymal epithelial cells and kidney explants. Kidney Int 70: 1607–1615, 2006. doi:10.1038/sj.ki.5001871. [PubMed: 16985513] [CrossRef: 10.1038/sj.ki.5001871]

7. Dijkman HB, Weening JJ, Smeets B, Verrijp KC, van Kuppevelt TH, Assmann KK, Steenbergen EJ, Wetzels JF. Proliferating cells in HIV and pamidronate-associated collapsing focal segmental glomerulosclerosis are parietal epithelial cells. Kidney Int 70: 338–344, 2006. doi:10.1038/sj.ki.5001574. [PubMed: 16761013] [CrossRef: 10.1038/sj.ki.5001574]

8. Discenza MT, He S, Lee TH, Chu LL, Bolon B, Goodyer P, Eccles M, Pelletier J. WT1 is a modifier of the Pax2 mutant phenotype: cooperation and interaction between WT1 and Pax2. Oncogene 22: 8145–8155, 2003. doi:10.1038/sj.onc.1206997. [PubMed: 14603255] [CrossRef: 10.1038/sj.onc.1206997]

9. Dressler GR, Deutsch U, Chowdhury K, Nornes HO, Gruss P. Pax2, a new murine paired-box-containing gene and its expression in the developing excretory system. Development 109: 787–795, 1990. [PubMed: 1977574]

10. Dressler GR, Woolf AS. Pax2 in development and renal disease. Int J Dev Biol 43: 463–468, 1999. [PubMed: 10535325]

11. Eccles MR, Wallis LJ, Fidler AE, Spurr NK, Goodfellow PJ, Reeve AE. Expression of the PAX2 gene in human fetal kidney and Wilms' tumor. Cell Growth Differ 3: 279–289, 1992. [PubMed: 1378753]

12. Fontaine F, Lecordier L, Vanwalleghem G, Uzureau P, Van Reet N, Fontaine M, Tebabi P, Vanhollebeke B, Büscher P, Pérez-Morga D, Pays E. APOLs with low pH dependence can kill all African trypanosomes. Nat Microbiol 2: 1500–1506, 2017. doi:10.1038/s41564-017-0034-1. [PMCID: PMC5660622] [PubMed: 28924146] [CrossRef: 10.1038/s41564-017-0034-1]

13. Friedman DJ, Kozlitina J, Genovese G, Jog P, Pollak MR. Population-based risk assessment of APOL1 on renal disease. J Am Soc Nephrol 22: 2098–2105, 2011. doi:10.1681/ASN.2011050519. [PMCID: PMC3231785] [PubMed: 21997396] [CrossRef: 10.1681/ASN.2011050519]

14. Gebeshuber CA, Kornauth C, Dong L, Sierig R, Seibler J, Reiss M, Tauber S, Bilban M, Wang S, Kain R, Böhmig GA, Moeller MJ, Gröne HJ, Englert C, Martinez J, Kerjaschki D. Focal segmental glomerulosclerosis is induced by microRNA-193a and its downregulation of WT1. Nat Med 19: 481–487, 2013. doi:10.1038/nm.3142. [PubMed: 23502960] [CrossRef: 10.1038/nm.3142]

15. Hayek SS, Koh KH, Grams ME, Wei C, Ko YA, Li J, Samelko B, Lee H, Dande RR, Lee HW, Hahm E, Peev V, Tracy M, Tardi NJ, Gupta V, Altintas MM, Garborcauskas G, Stojanovic N, Winkler CA, Lipkowitz MS, Tin A, Inker LA, Levey AS, Zeier M, Freedman BI, Kopp JB, Skorecki K, Coresh J, Quyyumi AA, Sever S, Reiser J. A tripartite complex of suPAR, APOL1 risk variants and $\alpha_v\beta_3$ integrin on podocytes mediates chronic kidney disease. Nat Med 23: 945–953, 2017. doi:10.1038/nm.4362. [PMCID: PMC6019326] [PubMed: 28650456] [CrossRef: 10.1038/nm.4362]

16. Herman-Edelstein M, Thomas MC, Thallas-Bonke V, Saleem M, Cooper ME, Kantharidis P. Dedifferentiation of immortalized human podocytes in response to transforming growth factor-β: a model for diabetic podocytopathy. Diabetes 60: 1779–1788, 2011. doi:10.2337/db10-1110. [PMCID: PMC3114395] [PubMed: 21521871] [CrossRef: 10.2337/db10-1110]

17. Husain M, Meggs LG, Vashistha H, Simoes S, Griffiths KO, Kumar D, Mikulak J, Mathieson PW, Saleem MA, Del Valle L, Pina-Oviedo S, Wang JY, Seshan SV, Malhotra A, Reiss K, Singhal PC. Inhibition of p66ShcA longevity gene rescues podocytes from HIV-1-induced oxidative stress and apoptosis. J Biol Chem 284: 16648–16658, 2009. doi:10.1074/jbc.M109.008482. [PMCID: PMC2713565] [PubMed: 19383602] [CrossRef: 10.1074/jbc.M109.008482]

18. Imasawa T, Obre E, Bellance N, Lavie J, Imasawa T, Rigothier C, Delmas Y, Combe C, Lacombe D, Benard G, Claverol S, Bonneu M, Rossignol R. High glucose repatterns human podocyte energy metabolism during differentiation and diabetic nephropathy. FASEB J 31: 294–307, 2017. doi:10.1096/fj.201600293R. [PMCID: PMC5161522] [PubMed: 27825100] [CrossRef: 10.1096/fj.201600293R]

19. Johnstone DB, Shegokar V, Nihalani D, Rathore YS, Mallik L, Ashish, Zare V, Ikizler HO, Powar R, Holzman LB. APOL1 null alleles from a rural village in India do not correlate with glomerulosclerosis. PLoS One 7: e51546, 2012. doi:10.1371/journal.pone.0051546. [PMCID: PMC3530541] [PubMed: 23300552] [CrossRef: 10.1371/journal.pone.0051546]

20. Kietzmann L, Guhr SS, Meyer TN, Ni L, Sachs M, Panzer U, Stahl RA, Saleem MA, Kerjaschki D, Gebeshuber CA, Meyer-Schwesinger C. MicroRNA-193a regulates the transdifferentiation of human parietal epithelial cells toward a podocyte phenotype. J Am Soc Nephrol 26: 1389–1401, 2015. doi:10.1681/ASN.2014020190. [PMCID: PMC4446868] [PubMed: 25270065] [CrossRef: 10.1681/ASN.2014020190]

21. Kopp JB, Nelson GW, Sampath K, Johnson RC, Genovese G, An P, Friedman D, Briggs W, Dart R, Korbet S, Mokrzycki MH, Kimmel PL, Limou S, Ahuja TS, Berns JS, Fryc J, Simon EE, Smith MC, Trachtman H, Michel DM, Schelling JR, Vlahov D, Pollak M, Winkler CA. APOL1 genetic variants in focal segmental glomerulosclerosis and HIV-associated nephropathy. J Am Soc Nephrol 22: 2129–2137, 2011. doi:10.1681/ASN.2011040388. [PMCID: PMC3231787] [PubMed: 21997394] [CrossRef: 10.1681/ASN.2011040388]

22. Kumar D, Plagov A, Yadav I, Torri DD, Sayeneni S, Sagar A, Rai P, Adabala M, Lederman R, Chandel N, Ding G, Malhotra A, Singhal PC. Inhibition of renin activity slows down the progression of HIV-associated nephropathy. Am J Physiol Renal Physiol 303: F711–F720, 2012. doi:10.1152/ajprenal.00643.2011. [PMCID: PMC3468493] [PubMed: 22718888] [CrossRef: 10.1152/ajprenal.00643.2011]

23. Lan X, Jhaveri A, Cheng K, Wen H, Saleem MA, Mathieson PW, Mikulak J, Aviram S, Malhotra A, Skorecki K, Singhal PC. APOL1 risk variants enhance podocyte necrosis through compromising lysosomal membrane permeability. Am J Physiol Renal Physiol 307: F326–F336, 2014. doi:10.1152/ajprenal.00647.2013. [PMCID: PMC4121568] [PubMed: 24899058] [CrossRef: 10.1152/ajprenal.00647.2013]

24. Lan X, Wen H, Lederman R, Malhotra A, Mikulak J, Popik W, Skorecki K, Singhal PC. Protein domains of APOL1 and its risk variants. Exp Mol Pathol 99: 139–144, 2015. doi:10.1016/j.yexmp.2015.06.003. [PMCID: PMC4509982] [PubMed: 26091559] [CrossRef: 10.1016/j.yexmp.2015.06.003]

25. Luna-Antonio BI, Rodriguez-Muñoz R, Namorado-Tonix C, Vergara P, Segovia J, Reyes JL. Gas1 expression in parietal cells of Bowman's capsule in experimental diabetic nephropathy. Histochem Cell Biol 148: 33–47, 2017. doi:10.1007/s00418-017-1550-z. [PubMed: 28315934] [CrossRef: 10.1007/s00418-017-1550-z]

26. Miesen L, Steenbergen E, Smeets B. Parietal cells–new perspectives in glomerular disease. Cell Tissue Res 369: 237–244, 2017. doi:10.1007/s00441-017-2600-5. [PMCID: PMC5487848] [PubMed: 28361304] [CrossRef: 10.1007/s00441-017-2600-5]

27. Mikulak J, Oriolo F, Portale F, Tentorio P, Lan X, Saleem MA, Skorecki K, Singhal PC, Mavilio D. Impact of APOL1 polymorphism and IL-1β priming in the entry and persistence of HIV-1 in human podocytes. Retrovirology 13: 63, 2016. doi:10.1186/s12977-016-0296-3. [PMCID: PMC5011791] [PubMed: 27599995] [CrossRef: 10.1186/s12977-016-0296-3]

28. Murer L, Caridi G, Della Vella M, Montini G, Carasi C, Ghiggeri G, Zacchello G. Expression of nuclear transcription factor PAX2 in renal biopsies of juvenile nephronophthisis. Nephron 91: 588–593, 2002. doi:10.1159/000065017. [PubMed: 12138259] [CrossRef: 10.1159/000065017]

29. Nassirpour R, Raj D, Townsend R, Argyropoulos C. MicroRNA biomarkers in clinical renal disease: from diabetic nephropathy renal transplantation and beyond. Food Chem Toxicol 98: 73–88, 2016. doi:10.1016/j.fct.2016.02.018. [PubMed: 26925770] [CrossRef: 10.1016/j.fct.2016.02.018]

30. Ohtaka A, Ootaka T, Sato H, Ito S. Phenotypic change of glomerular podocytes in primary focal segmental glomerulosclerosis: developmental paradigm? Nephrol Dial Transplant 17, Suppl 9: 11–15, 2002. doi:10.1093/ndt/17.suppl_9.11. [PubMed: 12386275] [CrossRef: 10.1093/ndt/17.suppl_9.11]

31. Ohtaka A, Ootaka T, Sato H, Soma J, Sato T, Saito T, Ito S. Significance of early phenotypic change of glomerular podocytes detected by Pax2 in primary focal segmental glomerulosclerosis. Am J Kidney Dis 39: 475–485, 2002. doi:10.1053/ajkd.2002.31391. [PubMed: 11877566] [CrossRef: 10.1053/ajkd.2002.31391]

32. Pavenstädt H, Kriz W, Kretzler M. Cell biology of the glomerular podocyte. Physiol Rev 83: 253–307, 2003. doi:10.1152/physrev.00020.2002. [PubMed: 12506131] [CrossRef: 10.1152/physrev.00020.2002]

33. Reiser J, Kriz W, Kretzler M, Mundel P. The glomerular slit diaphragm is a modified adherens junction. J Am Soc Nephrol 11: 1–8, 2000. [PubMed: 10616834]

34. Ryan G, Steele-Perkins V, Morris JF, Rauscher FJ 3rd, Dressler GR. Repression of Pax-2 by WT1 during normal kidney development. Development 121: 867–875, 1995. [PubMed: 7720589]

36. Saleem MA, O'Hare MJ, Reiser J, Coward RJ, Inward CD, Farren T, Xing CY, Ni L, Mathieson PW, Mundel P. A conditionally immortalized human podocyte cell line demonstrating nephrin and podocin expression. J Am Soc Nephrol 13: 630–638, 2002. [PubMed: 11856766]

37. Stieger N, Worthmann K, Schiffer M. The role of metabolic and haemodynamic factors in podocyte injury in diabetes. Diabetes Metab Res Rev 27: 207–215, 2011. doi:10.1002/dmrr.1164. [PubMed: 21309047] [CrossRef: 10.1002/dmrr.1164]

38. Suzuki T, Matsusaka T, Nakayama M, Asano T, Watanabe T, Ichikawa I, Nagata M. Genetic podocyte lineage reveals progressive podocytopenia with parietal cell hyperplasia in a murine model of cellular/collapsing focal segmental glomerulosclerosis. Am J Pathol 174: 1675–1682, 2009.

doi:10.2353/ajpath.2009.080789. [PMCID: PMC2671256] [PubMed: 19359523] [CrossRef: 10.2353/ajpath.2009.080789]

39. Torres M, Gómez-Pardo E, Dressler GR, Gruss P. Pax-2 controls multiple steps of urogenital development. Development 121: 4057–4065, 1995. [PubMed: 8575306]

40. Toska E, Roberts SG. Mechanisms of transcriptional regulation by WT1 (Wilms' tumour 1). Biochem J 461: 15–32, 2014. doi:10.1042/BJ20131587. [PubMed: 24927120] [CrossRef: 10.1042/BJ20131587]

41. Tzur S, Rosset S, Shemer R, Yudkovsky G, Selig S, Tarekegn A, Bekele E, Bradman N, Wasser WG, Behar DM, Skorecki K. Missense mutations in the *APOL1* gene are highly associated with end stage kidney disease risk previously attributed to the *MYH9* gene. Hum Genet 128: 345–350, 2010. doi:10.1007/s00439-010-0861-0. [PMCID: PMC2921485] [PubMed: 20635188] [CrossRef: 10.1007/s00439-010-0861-0]

42. Vanhamme L, Paturiaux-Hanocq F, Poelvoorde P, Nolan DP, Lins L, Van Den Abbeele J, Pays A, Tebabi P, Van Xong H, Jacquet A, Moguilevsky N, Dieu M, Kane JP, De Baetselier P, Brasseur R, Pays E. Apolipoprotein L-I is the trypanosome lytic factor of human serum. Nature 422: 83–87, 2003. doi:10.1038/nature01461. [PubMed: 12621437] [CrossRef: 10.1038/nature01461]

43. Woolf AS, Winyard PJ. Gene expression and cell turnover in human renal dysplasia. Histol Histopathol 15: 159–166, 2000. [PubMed: 10668206]

44. Xu B, Zeng DQ, Wu Y, Zheng R, Gu L, Lin X, Hua X, Jin GH. Tumor suppressor menin represses paired box gene 2 expression via Wilms tumor suppressor protein-Polycomb group complex. J Biol Chem 286: 13937–13944, 2011. doi:10.1074/jbc.M110.197830. [PMCID: PMC3077594] [PubMed: 21378168] [CrossRef: 10.1074/jbc.M110.197830]

Figures and Tables

Fig. 1.

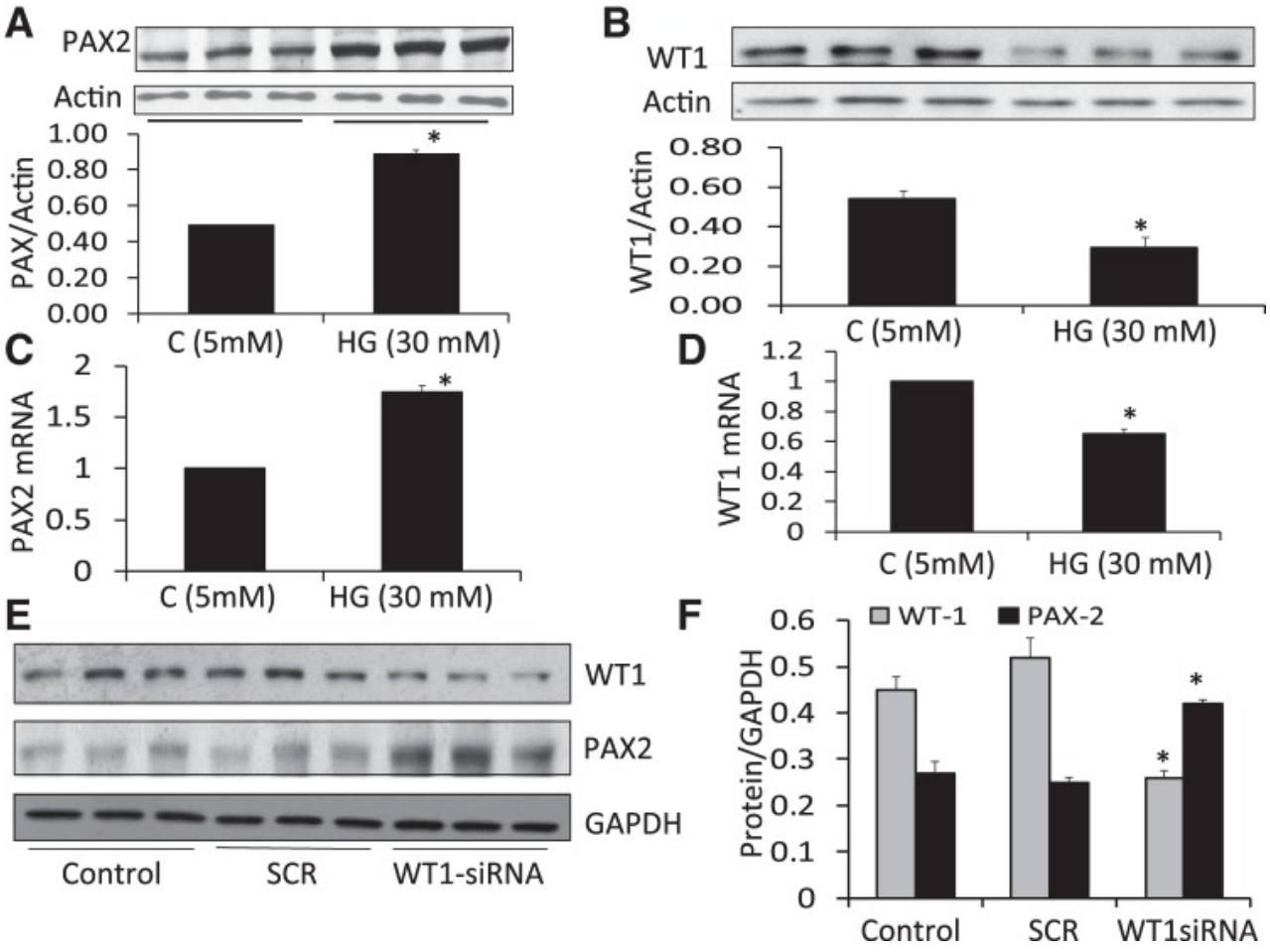

High glucose causes dedifferentiation of podocytes. *A*: differentiated podocytes [preincubated in RPMI 1640 media containing glucose (11 mM) at 37°C; DPDs] were incubated in media containing normal glucose (C; 5 mM) or high glucose (HG; 30 mM) for 48 h ($n = 3$). Proteins were extracted. Protein blots were probed for PAX2 and reprobed for actin. Gels from 3 different lysates are displayed (*top*). Cumulative densitometric data are shown in bar graphs (*bottom*). *$P < 0.05$ compared with C. *B*: protein blots from the lysate preparations of *A* were probed for WT1 and reprobed for actin. Gels from 3 different lysates are displayed. Cumulative data are shown in a bar diagram. *$P < 0.05$ compared with C. *C*: RNAs were extracted from the lysates of *A*. cDNAs were amplified with a specific primer for PAX2. Cumulative data on mRNA expression of PAX2 are shown. *$P < 0.05$ compared with C. *D*: RNAs were extracted from the lysates of *A*. cDNAs were amplified with a specific primer for WT1. Cumulative data on WT1 mRNA expression are shown. *$P < 0.05$ compared with C. *E*: DPDs were transfected with scrambled (SCR; 25 nM) or WT1 (25 nM) siRNAs with Lipofectamine RNAiMAX transfection reagent according to manufacturer's protocol and left in Opti-MEM for 48 h ($n = 3$). Subsequently, proteins were extracted, and protein blots from control and transfected cells were probed for WT1 and reprobed for PAX2 and GAPDH. Gels from 3 different lysates are displayed. *F*: cumulative densitometric data from the gels of *E* are shown in a bar diagram. *$P < 0.05$ compared with respective control and SCR.

Fig. 2.

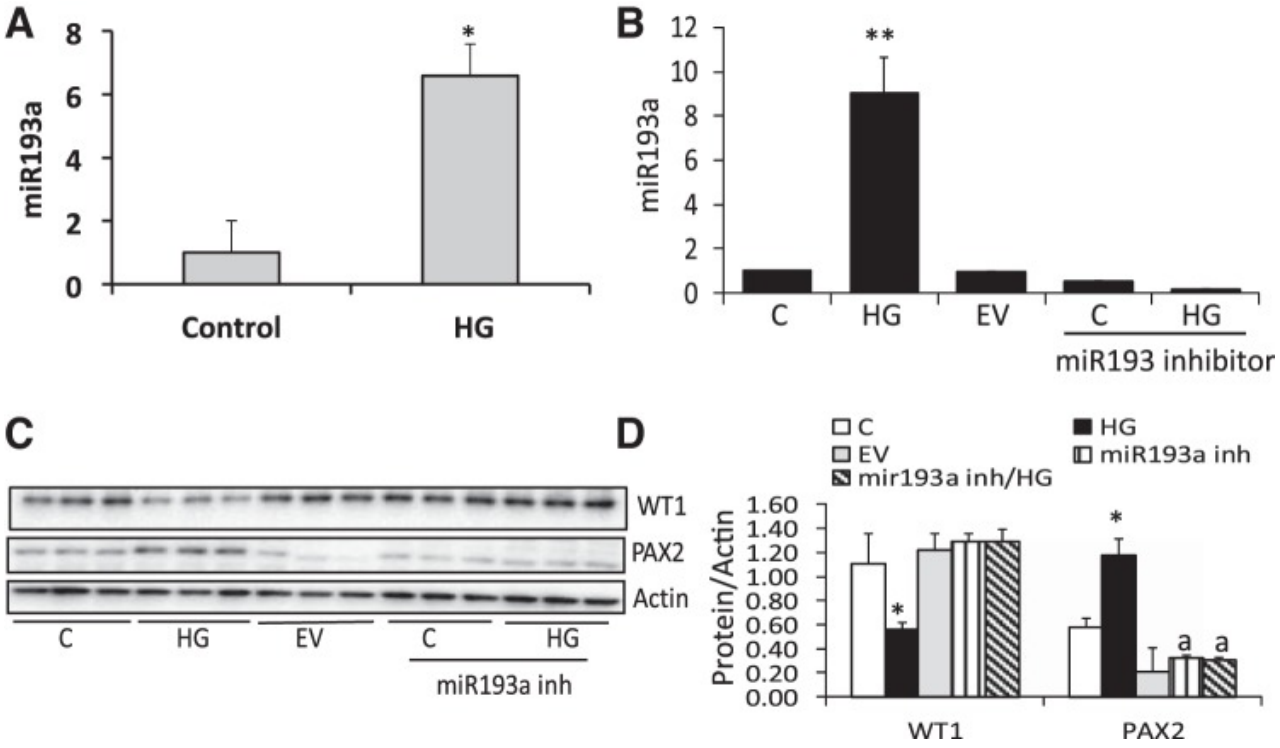

High glucose induces PD dedifferentiation through upregulation of miR193a. *A*: DPDs were incubated in media containing either normal glucose (control; 5 mM) or high glucose (30 mM) for 48 h ($n = 4$). RNAs were extracted and assayed for miR193a. Cumulative data are shown in a bar diagram. *$P < 0.05$ compared with C. *B*: DPDs were incubated in media containing normal glucose (5 mM; control), high glucose (30 mM), or empty vector (25 nM; pCMV-MIR; using Lipofectamine as a carrier) with or without miR193a inhibitor (25 nM; plasmid-based inhibitor using Lipofectamine as a carrier) for 48 h ($n = 3$). RNAs were extracted and assayed for miR193a. **$P < 0.01$ with other variables. *C*: DPDs were incubated in media containing normal glucose (control; 5 mM), high glucose (30 mM), or empty vector (EV; 25 nM) with/without a specific inhibitor (inh) of miR193a (25 nM; $n = 3$). After 48 h, proteins were extracted. Protein blots were probed for WT1 and reprobed for PAX2 and actin. Gels are displayed. *D*: cumulative densitometric data from the protein blots of *C*. *$P < 0.05$ compared with other WT1/PAX2 variables; $^{a}P < 0.05$ compared with respective C.

Fig. 3.

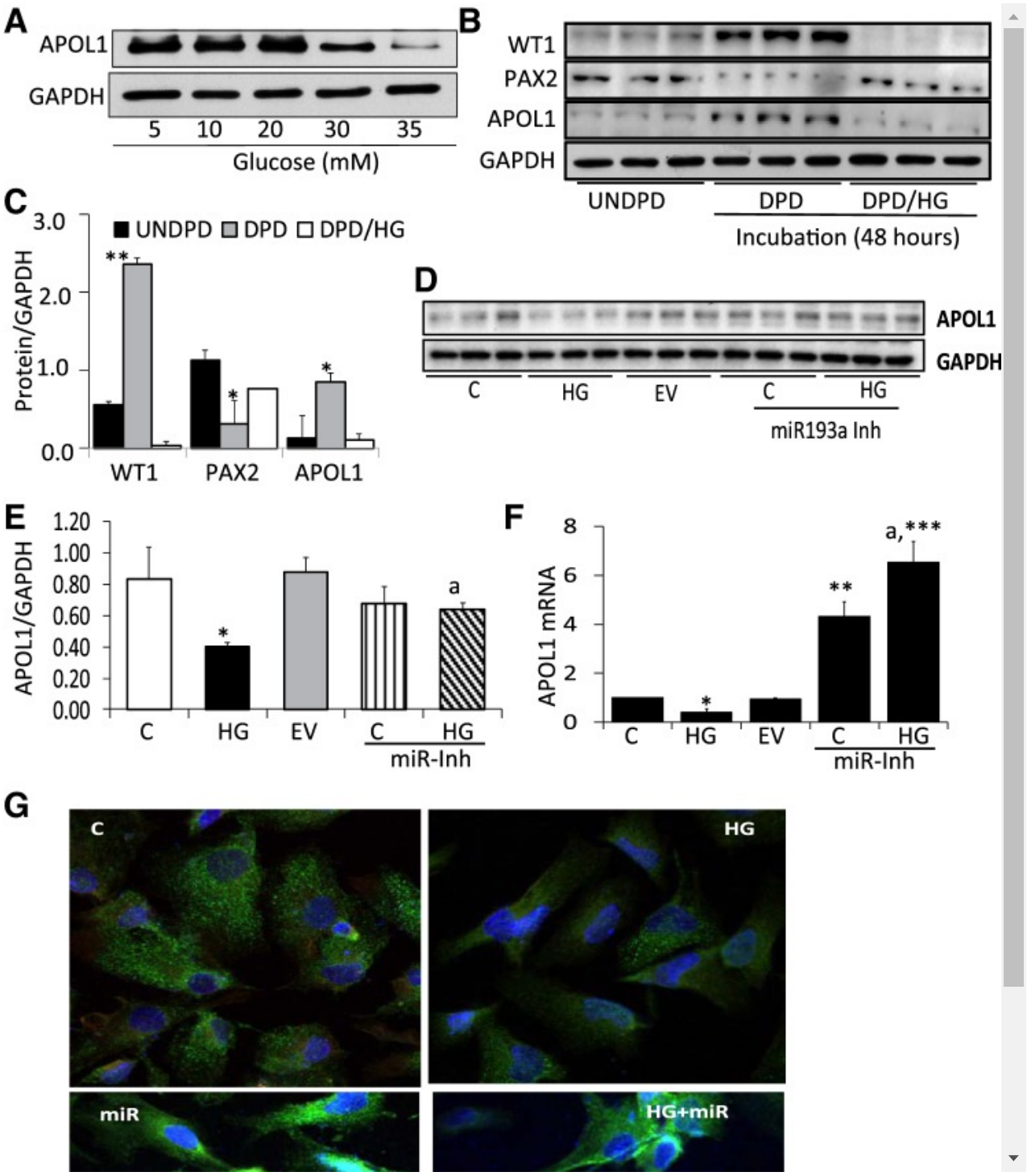

Open in a separate window

High glucose downregulates DPD expression of apolipoprotein (APO) L1 through upregulation of miR193a. *A*: DPDs were incubated in media containing different concentrations of glucose (5, 10, 20, 30, and 35 mM) for 48 h ($n = 3$). Protein blots were probed for APOL1 and reprobed for GAPDH. Representative gels are displayed. *B*: DPDs were incubated in media containing either conventional glucose (11 mM) or HG (30 mM) for 48 h. Proteins were extracted from UNDPDs and experimental DPDs ($n = 4$). Protein blots were probed for APOL1 and reprobed for WT1, PAX2, and GAPDH. Gels of 3 different lysates are displayed. *C*: cumulative densitometric data of protein blots of *B* are shown in a bar diagram. *$P < 0.05$ compared with respective UNDPD and DPD/HG; **$P < 0.01$ compared with respective UNDPD and DPD/HG. *D*: DPDs were incubated in media containing normal glucose (5 mM), high glucose (30 mM), or empty vector (25 nM) with or without miR193a inhibitor (25 nM; miR-Inh) for 48 h ($n = 3$). Proteins were extracted. Protein

blots were probed for APOL1 and reprobed for GAPDH. Gels are displayed. *E*: cumulative densitometric data are shown in bar graphs. **P* < 0.05 compared with C and empty vector (EV); [a]*P* < 0.05 compared with HG alone. *F*: RNAs were extracted from the lysate preparations of *D*, and cDNAs were amplified for *APOL1* mRNA. Cumulative data are shown in a bar diagram. **P* < 0.05 compared with respective C and EV; ***P* < 0.01 compared with C, EV, and HG alone; ****P* < 0.001 compared with C, EV, and HG alone; [a]*P* < 0.05 compared with miR-Inh alone. *G*: DPDs grown on coverslips were incubated in media containing either normal glucose (C) or high glucose with or without a miR193a inhibitor (miR; 25 nM) for 48 h (*n* = 3) followed by immunolabeling for APOL1. Subsequently, cells were examined under a confocal microscope. Representative fluoromicrographs are shown.

Fig. 4.

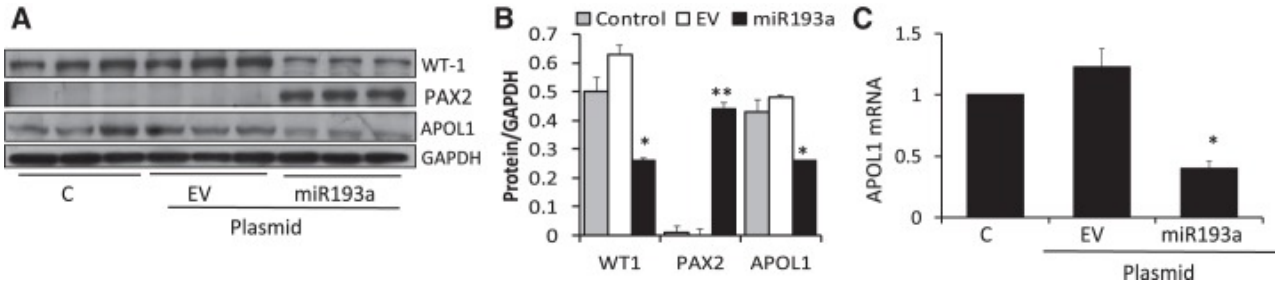

Overexpression of miR193a downregulates APOL1. *A*: DPDs were transfected with either empty vector (EV) or miR193a plasmid ($n = 3$). Proteins were extracted. Protein blots were probed for WT1, PAX2, and APOL1 and reprobed for GAPDH. Gels from 3 different lysates are displayed. *B*: cumulative densitometric data from the lysates of *A*. *$P < 0.05$ compared with control and EV; **$P < 0.01$ compared with control and EV. *C*: RNAs were extracted from the lysates of *A*. cDNAs were amplified with a specific primer for *APOL1*. *$P < 0.05$ compared with other variables.

Fig. 5.

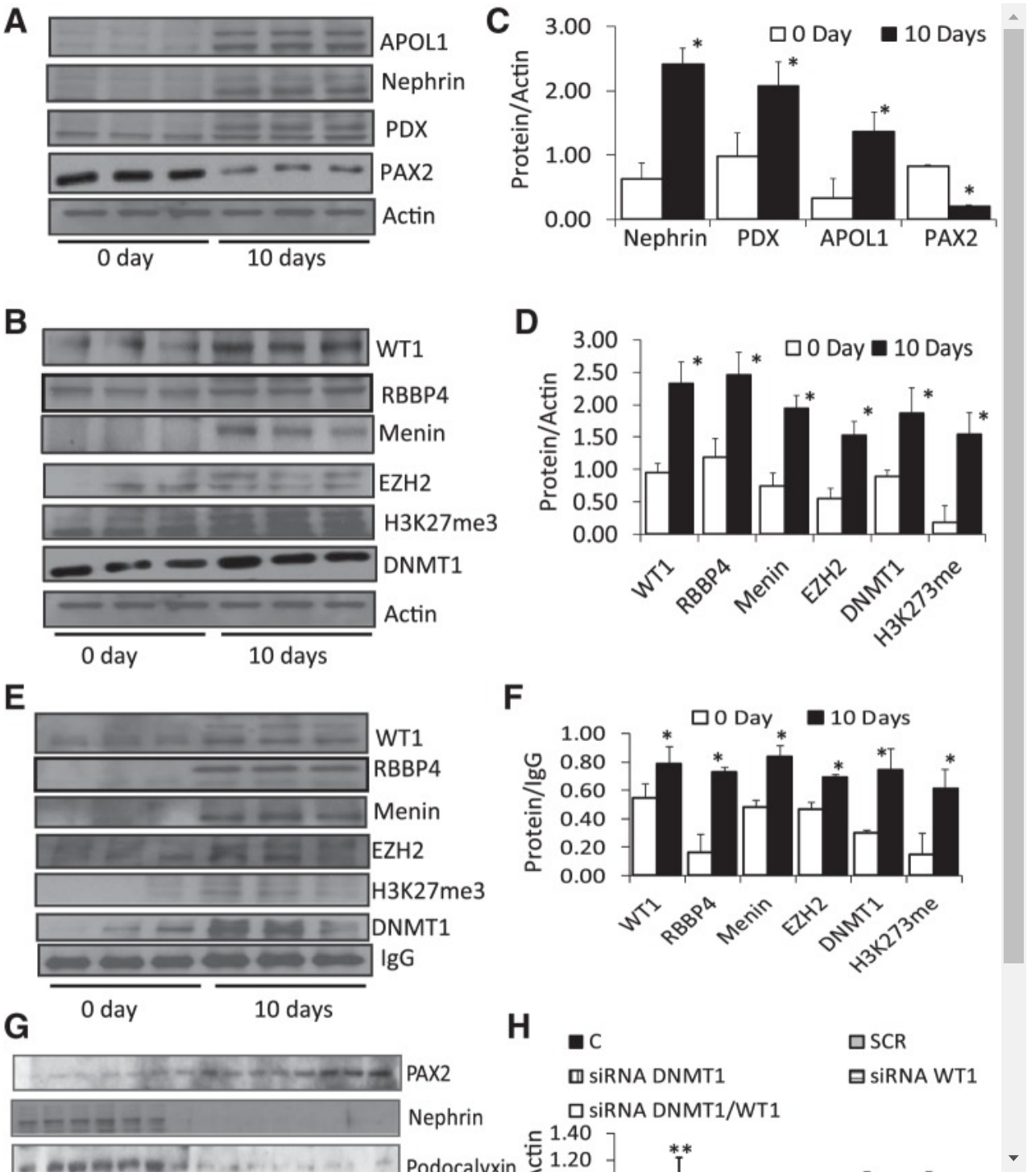

Open in a separate window

WT1 repressor complex preserves DPD molecular phenotype. *A*: protein blots of UNDPDs (0-day incubation) and DPDs (10-day incubation) were probed for PD (nephrin, WT1, and podocalyxin) and PEC (PAX2) markers, APOL1, and actin. Gels from 3 different lysates are displayed. *B*: protein blots from *A* were reprobed for the components of WT1 repressor complex. Gels from 3 different lysates are displaced. *C*: cumulative densitometric data from the lysates of *A* are shown as a bar diagram. **P* < 0.05 compared with respective 0-day. *D*: cumulative densitometric data from the lysates of *B* are shown as a bar diagram. **P* < 0.05 compared with respective 0-day. *E*: lysates from *A* were immunoprecipitated (IP) with the anti-WT1 antibody. IP fractions were probed for WT1, RBBP4 (Polycomb group protein), menin, H3K27me3, DNMT1, and IgG. Gels from 3 different IP fractions are displayed. *F*: cumulative densitometric data from the lysates of *E* are shown as bar graphs. **P* < 0.05 compared with respective 0-day. *G*: DPDs were transfected with scrambled (SCR),

WT1 siRNA (25 nM), DNMT1 (25 nM), or WT1 + DNMT1 siRNAs with Lipofectamine RNAiMAX transfection reagent according to manufacturer's protocol and left in Opti-MEM for 48 h (in WT1 + DNMT1 experiments, cells were exposed to WT1 siRNA for 48 h and DNMT1 siRNA for 24 h). Subsequently, proteins were extracted. Protein blots were probed for PAX2, WT1, nephrin, podocalyxin (PDX), and DNMT1 and reprobed for actin. Gels from 3 different lysates are displayed. *H*: cumulative densitometric data from the lysates of *G* are shown as a bar diagram. **P* < 0.05 compared with C, SCR, and DNMT1 siRNA in PAX2 variables; **P* < 0.05 compared with C, SCR, siRNA WT1 and siRNA DNMT1/WT1 in PDX and DNMT1 variables; ***P* < 0.01 compared with C, SCR, and DNMT1 siRNA in PAX2 variables; [a]*P* < 0.05 compared with C and SCR in nephrin variables; [b]*P* < 0.0.05 compared with C and SCR in PDX variables; [c]*P* < 0.01 compared C and SCR in WT1 variables; [d]*P* < 0.01 compared with DNMT1 siRNA, C, and SCR in DNMT1 variables.

Fig. 6.

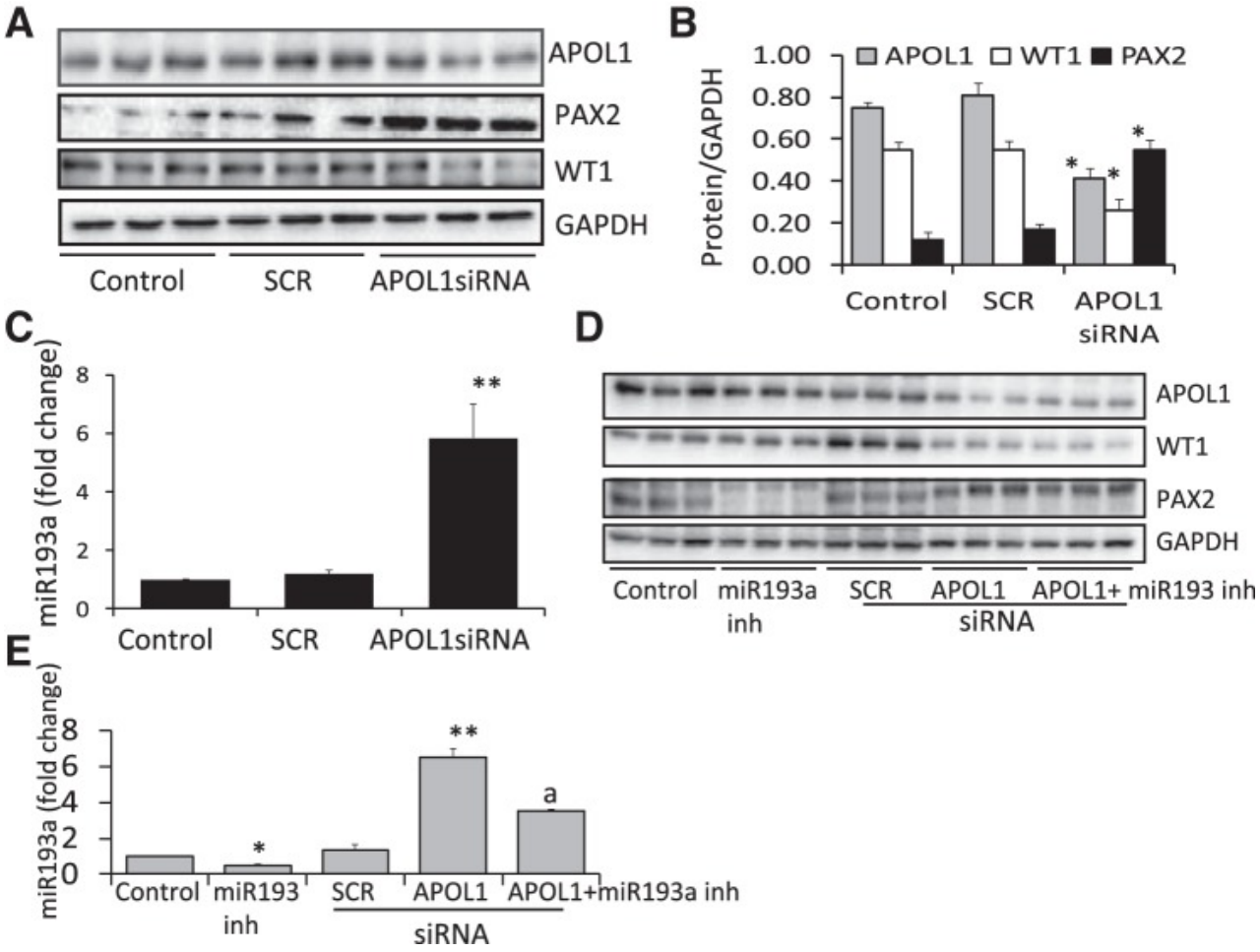

Role of APOL1 in preservation of DPD molecular phenotype. *A*: DPDs were transfected with either control (scrambled, SCR) or APOL1 siRNA. Proteins were extracted from control and transfected cells ($n = 3$). Protein blots were probed for APOL1 and reprobed for PAX2, WT1, and GAPDH. Gels from 3 different lysates are displayed. *B*: cumulative densitometric data of protein blots displayed in *A*. *$P < 0.05$ compared with respective APOL1, WT1, and PAX2 in control and SCR variables. *C*: DPDs were transfected with either control (scrambled, SCR) or APOL1 siRNA. RNAs were extracted from control and transfected cells ($n = 3$) and assayed for miR193a. Cumulative data are shown in a bar diagram. **$P < 0.01$ compared with other variables. *D*: DPDs were transfected with either control (scrambled, SCR) or APOL1 siRNA and incubated in media with or without miR193a inhibitor for 48 h ($n = 3$). Protein blots were probed for APOL1, WT1, PAX2, and GAPDH. Gels from 3 different lysates are displayed. *E*: RNAs were extracted from the lysate preparations of *D* and assayed for miR193a. Cumulative data are shown in a bar diagram. *$P < 0.05$ compared with control and SCR; **$P < 0.01$ compared with control, miR193a inh alone, and SCR; $^{a}P < 0.05$ compared with all other variables.

Fig. 7.

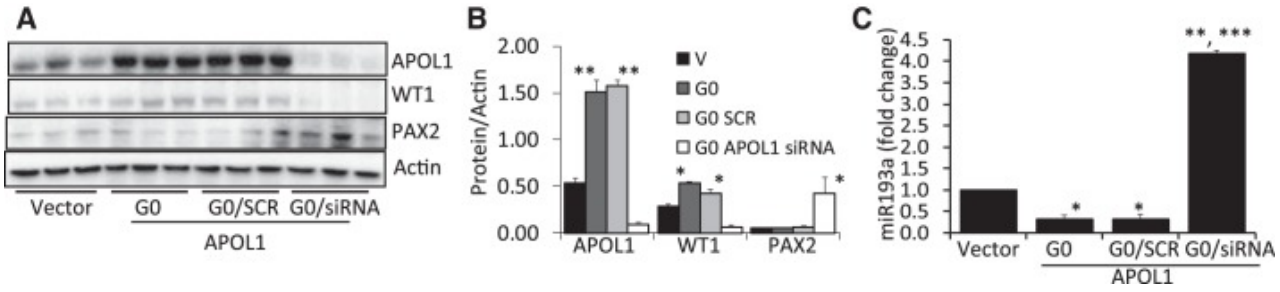

APOL1 negatively regulates miR193a expression in DPDs. *A*: UNDPDs stably expressing vector and overexpressing APOL1G0 were incubated in RPMI containing 11 mM glucose and 10% serum for 10 days at 37°C. APOL1G0-expressing DPDs were transfected with either scrambled or APOL1 siRNAs ($n = 6$). After 48 h, proteins were extracted from control (vector) and siRNA-transfected cells. Protein blots were probed for APOL1 and reprobed for WT1, PAX2, and actin. Representative gels from 3 different lysates are displayed. *B*: cumulative densitometric data ($n = 6$) from the protein blots of *A* are shown in a bar diagram. *$P < 0.05$ compared with vector (V) and G0 APOL1 siRNA in WT1 and all other variables in PAX2 proteins; **$P < 0.01$ compared with V and G0 APOL1 siRNA in APOL1 protein. *C*: RNAs were extracted from the lysates of *A*. RNAs were assayed for miR193a, and cumulative data are shown in a bar diagram. *$P < 0.05$ compared with vector; **$P < 0.01$ compared with vector; ***$P < 0.001$ compared with G0 and G0/SCR.

Fig. 8.

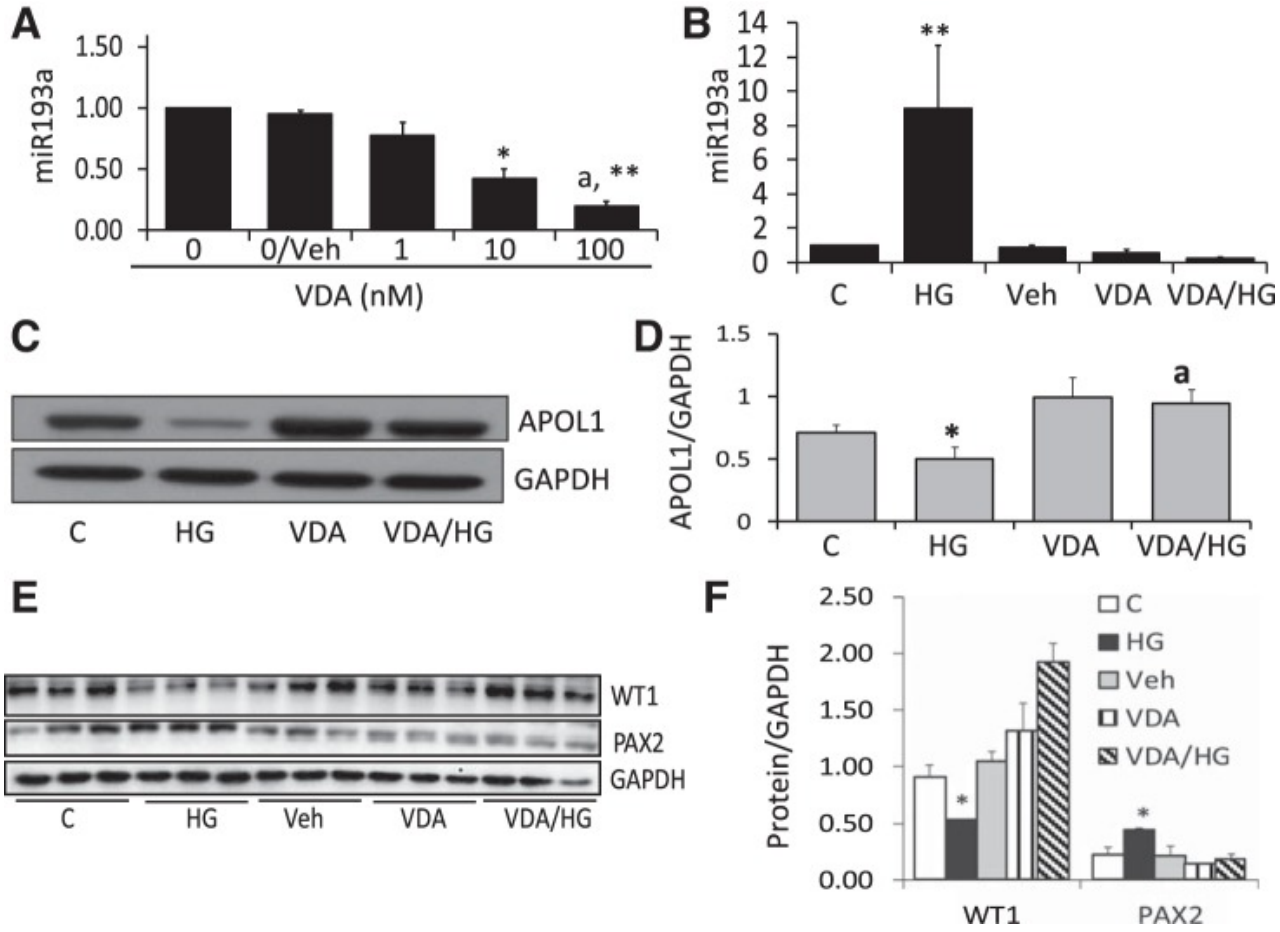

Vitamin D receptor (VDR) agonist (VDA) preserves DPD phenotype through modulation of miR193a-APOL1 axis in high-glucose milieu. *A*: UNDPDs were incubated in media containing either vehicle (0.1% DMSO) alone or different concentrations of VDA (EB 1089; 0, 1, 10, and 100 nM) for 48 h ($n = 3$). RNAs were extracted and assayed for miR193a. Cumulative data are shown in a bar diagram. *$P < 0.05$ compared with vehicle (VDA; 0 nM), VDA, 0 and 1.0 nM; **$P < 0.01$ compared with vehicle (VDA; 0 nM), VDA, 0 and 1.0 nM; $^{a}P < 0.05$ compared with VDA, 10 nM. *B*: DPDs were incubated in media containing normal glucose (C; 5 mM), high glucose (HG; 30 mM), or vehicle (0.1% DMSO) with or without VDA (EB 1089; 10 nM) for 48 h ($n = 3$). RNAs were extracted and assayed for miR193a. Cumulative data are shown in a bar diagram. **$P < 0.01$ compared with other variables. *C*: DPDs were incubated in media containing either normal glucose (C; 5 mM) or high glucose (HG; 30 mM) with or without VDA (EB 1089; 10 nM) for 48 h ($n = 3$). Protein blots were probed for APOL1 and reprobed for GAPDH. Representative gels are displayed. *D*: cumulative densitometric data from the lysates of *C* are shown in a bar diagram. *$P < 0.05$ compared with C; $^{a}P < 0.05$ compared with HG alone. *E*: DPDs were incubated in media containing normal glucose (C; 5 mM), vehicle (Veh; 0.1% DMSO), or high glucose (HG; 30 mM) with or without VDA (EB 1089; 10 nM) for 48 h ($n = 3$). Protein blots were probed for WT1 and PAX2 and reprobed for GAPDH. Representative gels are displayed. *F*: cumulative densitometric data from the protein blots of *E* are shown in a bar diagram. *$P < 0.05$ compared with respective all other variables.

Fig. 9.

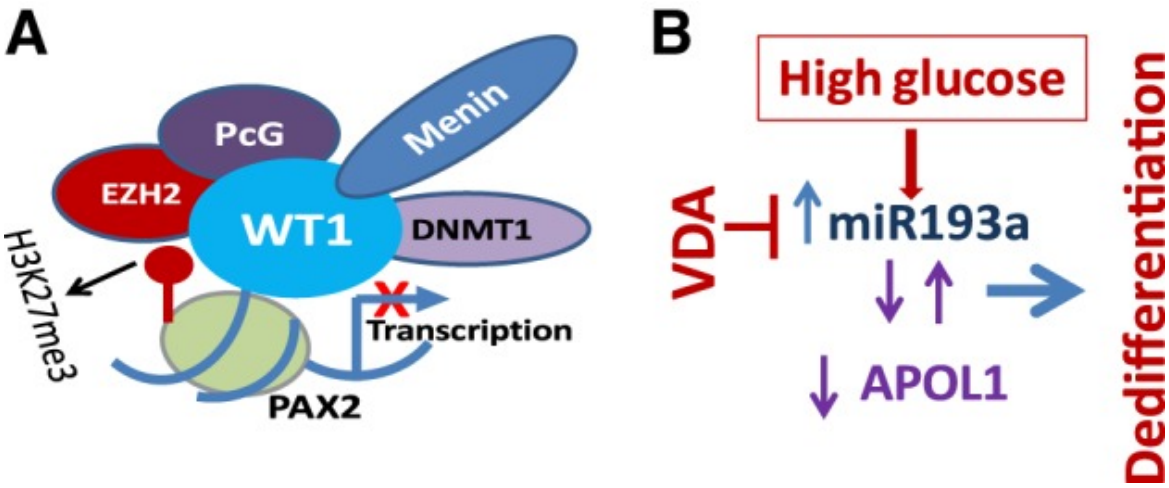

Proposed mechanistic schemes. *A*: composition of WT1 repressor complex is shown in a cartoon. WT1 repressor complex binding to PAX2 promoter represses its transcription. Disruption of this complex would derepress the expression of PAX2. *B*: high glucose enhanced the expression of miR193a, which led to downregulation of APOL1 expression in DPDs. These alterations in miR193a-APOL1 axis induced DPD dedifferentiation. VDA provided protection against this effect of high glucose through the reversal of miR193a-APOL1 axis alterations. PcG, Polycomb group.